Proceedings of the 11th ICPMG 2026
11th International Conference on Physical Modelling in Geotechnics
8-12 June 2026, Zurich, Switzerland

1g and Centrifuge scaled modelling of embedded mooring lines for deployment of a novel offshore anchoring system in rock strata

Thomas Riccio[1], Rachael Smith[2], Karlis Caucis[1], Philip Strong[2], Peter Shiner[2], Matteo Alessandri[1], Hamed Noori[1], Michael J. Brown[3], Craig Davidson[3]

[1]*Global Maritime, Newcastle upon Tyne, United Kingdom, thomas.riccio@globalmaritime.com*

[2]*Reflex Marine, Cornwall, United Kingdom, rachael.smith@reflexmarine.com*

[3]*University of Dundee, Dundee, United Kingdom, m.j.z.brown@dundee.ac.uk*

ABSTRACT: This paper investigates the performance of embedded line mooring systems, studied as part of the development of a new novel anchor technology intended to target deep water and variable geotechnical strata. The Javelin anchor system (JAS) features an embedded tether mooring line (JTA, the Javelin tether assembly) which transmits load to a deep-set anchor (JUA and JLA, the Javelin upper and lower anchors respectively). Building on a series of lab-floor 1g tests exploring the JTA, large deformation centrifuge tests at representative field stress levels are planned to be performed at the University of Dundee. The centrifuge tests seek to better understand load-shedding characteristics of the JTA, improve the embedded mooring line design approach planned to model the JTA, verify the applicability of the 1g tests, as well as widen the industries knowledge regarding embedded line-soil interactions. This paper will describe findings from the existing 1g JTA test series, compare with existing methodologies recommended for offshore tether design, as well as outline the motivations around the planned centrifuge programme and its associated goals. The centrifuge programme also hopes to address a need for quantification of the cyclic behaviour of embedded mooring lines, which is also a key design consideration for the JAS.

1 INTRODUCTION

To meet the requirements of the Paris Agreement, a global goal of achieving 380 GW of offshore wind by 2030 has been proposed by the Offshore Wind Energy Compact (Cerfontaine, et al., 2023; IRENA and GWEC, 2024). To facilitate this, offshore renewable energy is trending towards deeper water where floating-type assets (FLOW) moored to the seabed are opted for over traditional fixed-bottom solutions. In these cases, multi-line mooring systems (catenary, taut or semi-taut type) are affixed to a FLOW and transmit environmental, and ocean loads to a seabed gravity-based or embedded foundation solution (e.g., drilled and grouted piles, suction anchors, drag embedment anchors).

Following whole-life geotechnical design philosophy (Gourvenec, 2020), fabrication, installation, operation and decomissioning phases of an offshore anchor contribute markedly to its overall sustainability. Efficient anchoring solutions with small environmental footprints and installation costs are therefore encouraged as the industry moves toward deeper waters and more challenging loading conditions.

Reflex Marine (RM) are currently developing a new foundation technology called the Javelin Anchor System (JAS) which aims to address those criteria; a deep-set/bore drilled and grouted composite anchor attached to a flexible tether line (Javelin tether assembly, JTA, Figure 1a). The JAS intends to augment design features from other proven technologies (e.g., drilled and grouted anchors, embedded mooring line systems) but seeks to optimise material and installation requirements through careful sizing of the deep-set anchor component. This will entail a two-step diameter profile comprised of an upper- and lower anchor unit (i.e., the Javelin Upper Anchor (JUA) and Javelin Lower Anchor (JLA)) which shall be embedded within the rock stratum (Figure 1a).

The JAS is intended for deployment in a wide range of offshore environments including water depths of between 50-120 m, and at sites with rock stratigraphy combined with shallow- or deep overlying superficial deposits. For instances where sufficient superficial deposits are present (e.g., >5 m), the deep-set anchor shall be configured with the JTA component. This aims to further optimise requirements of the JUA and JLA by shedding loads transmitted to the JUA pad-eye from the mooring load connector (MLC) above the mudline (Figure 1a). For the JTA, work is currently ongoing to optimise its requirements, which will inform the sizing envelopes of the JUA and JLA, forming part of the DNV technical qualification process. This work entails verifying different JTA configurations and their efficiency at shedding load (specifically, large lateral loads) transmitted to the JUA as well as their performance under long-term cyclic loading. To do this, alongside various parametric-type sizing studies, RM have also conducted a series of 1g 1:10 scale model physical tests of JTA configurations (as arranged in Figure 1b). This paper will describe the set-up of those as well as findings from the test series. Other studies relating to the JLA/JUA are planned/ongoing.

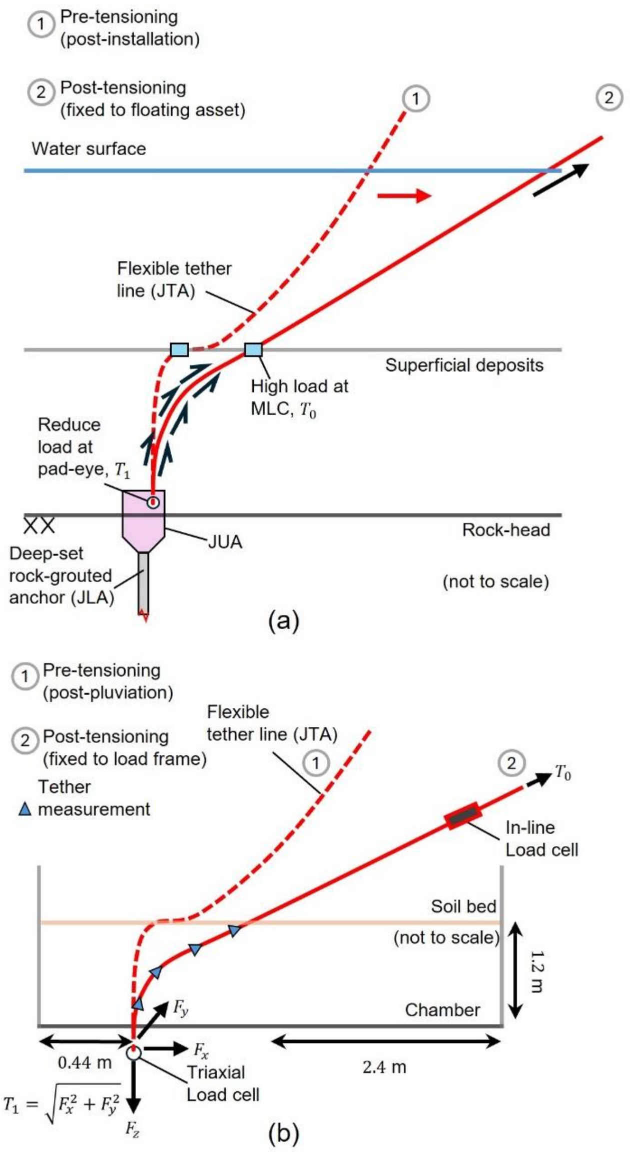

Figure 1. (a) Schematic of JTA mooring line and deep-set JUA and JLA anchor system for a floating offshore asset following (1) installation and (2) following application of pretension (T_0); and (b) 1g & centrifuge model JTA set-up

This paper will also review applicability of the findings through predictions made using full-scale design frameworks by Mortensen et al. (2015); Frankenmolen et al. (2016) and Kwa et al. (2025). This review seeks to highlight any limitation of the 1g tests. Building on above are a series of large-deformation centrifuge tests which are planned to be performed at the University of Dundee. The centrifuge programme, its motivations and goals are also described herein.

2 1G MODEL TEST SERIES

The small-scale 1g model test series of the JTA set-up (as schematised in Figure 1b) was undertaken at the Javelin test centre facility in Bristol, description around the set-up is given below. Results are described from the 1:10 scale testing programme to allow comparison with existing numerical methods and their relevance/motivation behind the planned centrifuge programme, see Table 1.

Table 1. Summary of example tests from test series

Test Phase No.	Loading
5_1	Monotonic (ramped 2500 N inc to 9900 N)
5_2	
5_1 (cyclic)	Cyclic (10 cycles @ 0-9900 N)
5_2 (cyclic)	

2.1 JTA test set-up

Precast concrete blocks were used to form a chamber with internal dimensions of $W_{chamber}$ x $L_{chamber}$ x $H_{chamber}$ 0.6 x 4.8 x 1.2 m (Figure 1b; Figure 2a). At the base of the chamber, a pad-eye connection point with a multi-directional PCM ± 40 kN pancake tri-axial load cell was positioned. As the goal of the tests was to assess load shed characteristics of the JTA only, the JUA/JLA were considered as a fixed point at the base of the sand bed (see e.g., Figure 1b) and the rock bed was not explicitly modelled. Load shed was measured through an in-line load cell (Figure 1b; Figure 2a) whilst profiling of the embedded line was achieved via four vertical measurement probe lines fixed along the embedded wire (e.g., see blue triangles Figure 1b, Figure 2b).

2.1.1 Model scaling, tether properties and mooring load assumptions

Sizing followed scaling laws initially proposed by Brown et al. (2006) for ploughing experiments, recently validated by centrifuge testing by Robinson et al., 2019 & Shariff et al., 2024. A 0.012 m diameter spiral strand wire manufactured by Certex was used to perform the tests, its minimum breaking strength was 140.6 kN; well within that planned for the test series (<10 kN).

Loading values are summarised in Table 2 and were assumed to be analogous to those anticipated for a 6-line semi-taut mooring system for a FLOW. It was also assumed that the loads presented were inclusive of any mean and dynamic loading and any relevant safety factors prescribed for floating offshore wind in DNV-ST-0119 (2021).

Table 2. Model scaling for 1g test series (N=10)

Property	Model scale	Prototype (field)
Tether diameter, $\boldsymbol{D}$ [m]	0.012	0.12 ($D \cdot N$)
Tether weight (in air), $\boldsymbol{w_L}$ [kN/m]	0.007	0.7* ($w_L \cdot N^2$) *taken as 0.45 based on typical values
Maximum tension load, $\boldsymbol{T_0}$ [kN]	9.9	9900 ($T_0 \cdot N^3$)

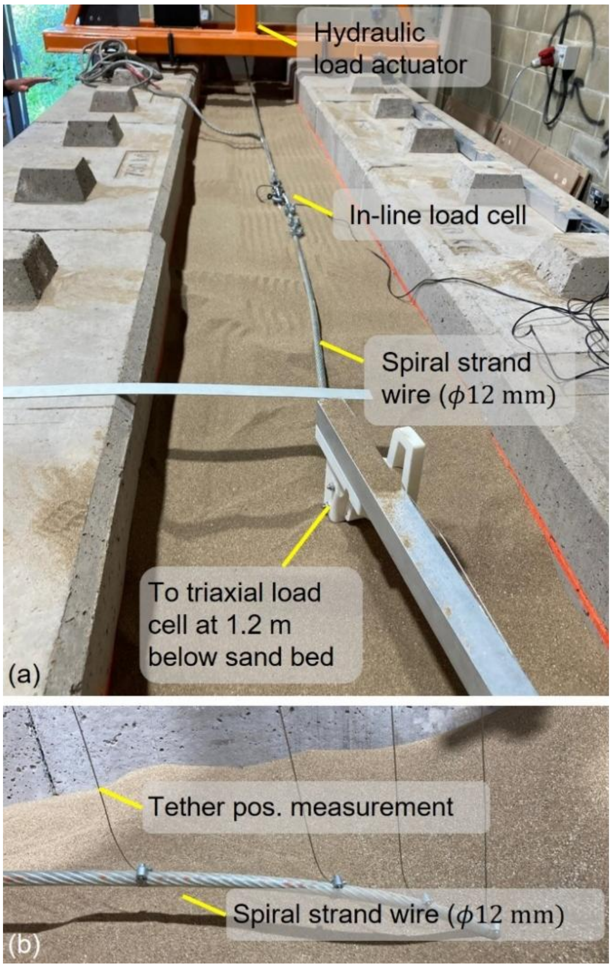

Figure 2. Large-scale 1g experimental tests at RM HQ showing: (a) Sand-bed chamber/pre-testing and (b) tether line and position measurements

2.1.2 Sand and grain-scaling and boundary conditions

Unsaturated medium-dense beds of cornish-lime marine sand (CLS-37) were prepared. Properties of the CLS-37 sand are provided in Table 3 and its PSD is shown in Figure 3. For the planned centrifuge programme described later, HST-95 sand is expected to be used; its properties too are summarised in Table 3 and its PSD curve is overlain in Figure 3. CLS-37 has a marginally larger mean grain-size (d_{50}) than the HST-95 fine sand but both have a similar degree of sorting and an effective particle size of ~0.1 mm. For the 1g tests herein, the CLS-37 sand satisfied typical rule-of-thumb criterion for grain-scaling: $D/D_{50} \approx 36$ with grain-scaling issues generally being avoided where $D/D_{50} > 20$, after Bolton et al. (1999). Criterion vary depending on structure and load application and grain-scaling shall be explored further prior to future testing.

Table 3. Sand properties for 1g and centrifuge tests

Property	CLS-37	HST-95
Average particle size, $\boldsymbol{d_{50}}$ [mm]	0.33	0.14
Effective particle size, $\boldsymbol{d_{10}}$ [mm]	0.10	0.09
Particle specific gravity [-]	~2.63	2.63
Minimum dry density [$\mathbf{Mg/m^3}$]	1.43	1.459
Maximum dry density [$\mathbf{Mg/m^3}$]	1.73	1.758
Approx. dry unit weight [kN/m^3]	15	16
CS friction angle, $\boldsymbol{\phi}$ [°]	32	32

The finer HST-95 sand for the planned centrifuge tests is preferred given that the JTA's diameter will be significantly smaller, such to achieve similtude, more information is given in Section 3. Interface measurments to confirm roughness and any scaling limitations (e.g., perfectly rough, perfectly smooth or intermediate conditions) are ongoing and platen-interface testing representing steel-tether conditions are anticipated, noting relevant discussions around chain/sand-sand interactions by Rui et al. (2021).

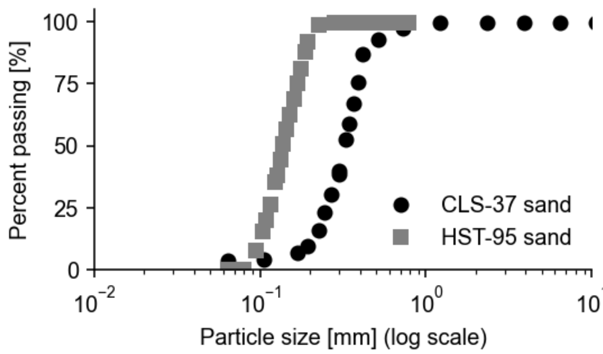

Figure 3. Particle size distribution for the 1g tests (CLS-37) and HST-95 intended for the centrifuge test programme

2.1.3 Sand bed preparation

Sand beds were prepared through air pluviation. This was facilitated with a new 4-tonne top-loaded hopper developed by RM. The pluviator was paired with a variable gauze adapter which could be adjusted for different density requirements and sand gradings, a finer gauze mesh below the hopper was also used to prevent despersion/over-sorting of grains. The pluviator to sand-bed top exceeded the height necessary to achieve terminal velocity and thus a consistent placement rate at all stages of the pluviation was assumed. During pluviation, the model JTA was held in position one (vertically) as schematised before in Figure 1b, this broadly represented the status of the anchor following bore-drilling, installation and prior to any JTA pretension application. Whilst no provision was made to model a mud-supported bore around the JTA, the impact on the overall response was expected to be limited, given the large-deformation experienced by the tether during pretension. Samples were intended to be medium density ($D_r \approx 55\%$). Macro post-test measurements indicated that $D_r \approx 60 \pm 5\%$.

2.1.4 Boundary effects

To avoid excessive boundary effects relating to stress-field interactions within the model container, centre-to-centre distances to any boundary should, as a rule-of-thumb, exceed $L/_D \approx 10 - 50$ (Albiker et al., 2017; Schnaid & Houlsby, 1991). Since $L_{chamber}/_D > 110$ and $W_{chamber}/_D > 50$, marked boundary effects were generally not anticipated.

2.1.5 JTA testing procedure

Load increments were applied above the sand bed in-line with the JTA via a hydraulic actuator (controlled by a FLOWIT monoblock directional control valve). Load was ramped in four no. increments of approximately 2500 N, up to a maximum of 9900 N. This was well within the permissible limits of the actuator and load cell arrangement. At tension loads approaching 9900 N it was assumed that the JTA resembled a catenary mooring line and could be discussed in line with associated design frameworks, as done later in Section 0.

2.2 Results and discussion

Inverse catenary mooring line performance characteristics are usually assessed by numerical integration of the following equilibrium equations:

$$\frac{dT}{ds} = F + W'_l \cdot sin\theta \qquad (1)$$

$$T\frac{d\theta}{d_s} = -N + W'_l \cdot cos\theta \qquad (2)$$

Where T is the tether tension load; θ is the tether angle with respect to the horizon, s is the distance along the chain length; F is the frictional resistance per unit length of the tether at the soil-tether interface; N is the soil's bearing resistance per unit length of the tether (normal to its current inclination), W'_l is the tether's submerged unit weight.

These were originally defined in Neubecker & Randolph (1995), recognised in DNV-RP-E302 (2021) and are typically implemented with various bearing-capacity-based formulae (Mortensen et al., 2015). For a drained scenario, F and N may be estimated through modified strip footing formulae where:

$$N = D \cdot A_{sand} (N_q \cdot \sigma'_v + 0.5 \cdot D \cdot A_{sand} \cdot \gamma' \cdot N_\gamma) \qquad (3)$$

Where bearing capacity factors are:

$$N_q = e^{\cdot\pi} \cdot tan\phi \cdot \tan^2\left(45 + \frac{\phi}{2}\right) \qquad (4)$$
$$N_y = (N_q - 1) \cdot \tan(1.4\phi)$$

Where:

$$F = Q \cdot \tan\delta' \qquad (5)$$

Where ϕ is the soil's friction angle; $\tan\delta'$ is assumed to be the soil-tether interface coefficient (in this instance, taking a median estimate as $\delta' = 0.75 \cdot \phi$); σ'_v is the effective soil overburden pressure; and A_{sand} is an empirical adjustment factor used to scale the effective bearing area (usually taken as $A_{sand} = 1$ for a wire (Kwa et al., 2025; Mortensen et al., 2015)). More recently, Frankenmolen et al. (2016) developed empirical expressions linking F and N with cone resistance formulae (e.g., $N = D \cdot A_b \cdot \beta \cdot q_c; F = D \cdot A_s \cdot \zeta \cdot q_c = \mu \cdot N$) where β and ζ are replacement scaling factors for the bearing capacity and interface formulae introduced above, where μ is the frictional coefficient reported as $\mu \approx 0.25$. Kwa et al. (2025) recognised that the tether inclination (θ) curtails the limiting N and F which was not considered in the original CPT approach developed by Frankenmolen et al. (2016). Accordingly, authors incorporated θ dependence on the bearing contributions through the analogy of a laterally loaded pile and its associated limited lateral loading pressures. The function essentially recognised that as a tether tends to the vertical, its ability to shed load diminishes (e.g., contributions of F and N reduce), e.g., $\beta(\theta = 90) \ll \beta(\theta = 0)$.

2.3 Application to the 1g test results

Prototype tether profiles for static tests 5_1 and 5_2 at peak pretension ($T_0 \approx 9.9$ MN) are shown in Figure 4a. Figure 4b and c show each tests' load-shedding performance by comparing load T_0 with that at the pad-eye, T_1, and its associated inclination (θ) for the four applied loading increments, respectively. Results are shown alongside the three empirical methods introduced above.

2.4 Discussion

Noting possible limitations of the 1g tests appreciated below, none of the empirical methods were able to replicate the full mooring profile of test 5_1 and 5_2 at peak tension ($T_0 = 9.9$ MN) (Figure 4a). Whilst Mortensen's method captured reasonably well the peak horizontal displacement (Figure 4a), and tether inclination at the pad-eye (Figure 4b), its reliability to estimate inclination throughout the profile varied. At the sand-bed surface, both Kwa and Frankenmolen's CPT-based methods underestimated the total horizontal distance of the tether more significantly than Mortensen's method.

Regarding estimation of the inclination angle (θ) at the pad-eye, Frankenmolen and Kwa's CPT methods indicated an average error of 23% and 4%, respectively, whilst Mortensen's method differed from tests 5_1 and 5_2 by 6%. Better performance of Kwa's method likely stemmed from its inclusion of tether inclination on mobilised resistance, recognisable by comparing to Frankenmolen's method, which estimated far greater bearing contributions and clear verticalisation of the tether in proximity to the pad-eye.

For load-shedding predictions, Kwa's CPT method was most effective at back-predicting tests 5_1 and 5_2, with an error of 5% across the load range applied at the sand-bed (Figure 4c). Frankenmolen's CPT method indicated an average error of 14%, whilst Mortensen's method indicated the greatest variation at 24%, both becoming more marked with increasingly high pretension. The average overall better performance from Kwa's method across the load range applied may again be attributed to reasons described above. The better performance of the CPT methods in general might have been linked to their calibration using other finite-sized model tests. CPT profiles used here were based upon the average relative density of the sand bed ($R_d \approx 62\%$) applied to a synthetic CPT-profile formulation, developed from other small-scale tests (Baldi et al., 1983).

Cyclic results 5_1c and 5_2c are superimposed in Figure 4b and c. These showed that tether inclination at the pad-eye reduces as horizontal displacement accumulates toward the pretension direction. Counterintuitively, the expected load transmitted to the pad-eye reduced. This may have been related to local densification/stiffening of the sand bed, a mechanism previously observed for laterally cyclically loaded piles in loose sand (Basak et al., 2022). An increased effective reaction area (e.g., $A_{sand} > 1$) related to increasing embedment of the tether and interlocking of grains around the spiral strand wire may also have played a role.

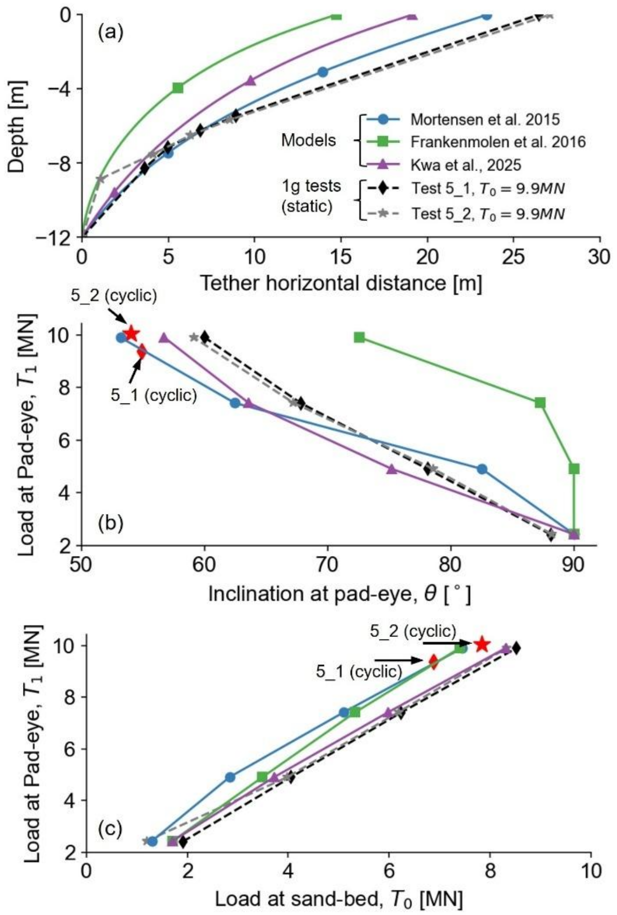

Figure 4. Modelled results versus static 1g experimental results (prototype scale) showing: (a) embedded JTA profiles at peak load; (b) JTA angle at the pad-eye versus current load at sand-bed surface; and (c) JTA load shedding (load at the sand bed versus load at the pad-eye)

Despite the empirical methods reasonably back-predicting elements of the JTA performance, the 1g tests appeared to be influenced by stress levels and possible boundary effects. For example, the general increase in gross-error between the experimental results close to the sand-bed surface may have been caused by the increasingly low stress levels associated with the 1g set-up, rather than the methods themselves. Subsequently, the reconciliation of error toward the pad-eye (e.g., load-shed and angle, Figure 4b, c) may partly have stemmed from the boundary effects (increased normal and shear resistances not expected at the associated proto-type depth) caused by interaction with the container base, as well as a general increase in the in-situ stress level. Full-scale or centrifuge prototype tests would therefore be valuable to quantify these effects. Furthermore, both the static and cyclic tests were conducted in dry sand under drained conditions and whilst all methods described above are suited to drained-type analyses, the performance characteristics may not be representative of field-scale conditions where increasingly undrained conditions might be expected.

3 PLANNED CENTRIFUGE TESTING PROGRAMME

Tests at the University of Dundee will be performed using the Actidyn C67-2 geotechnical centrifuge. Four phases of testing of the JTA are planned and include both static and cyclic testing as summarised in Table 4. Phase 1 tests seek to verify the applicability of the existing 1g tests to estimate load shedding and profile characteristics of the JTA as well as supporting the validation and application of existing mooring analyses methods discussed in Section 0. Phases 2 to 4 hope to quantify the effect of: (a) saturation (e.g., buoyancy and changes to the geostatic stress level throughout the sand-bed on the JTA response); and (b) partial 1-way cyclic loading on the JTA's performance (e.g., its overall ability to reduce transmittable forces to the pad-eye under adverse conditions expected in an offshore environment). Whilst the 1g tests explored cyclic conditions, these were performed within dry sand beds where the effects of excess pore pressure generation were ignored. With that in mind, the centrifuge tests will be configured for both drained and undrained testing to identify any appreciable effects.

Table 4. High-level summary of planned centrifuge tests

Phase	Drainage	Density	Load
1.1	Dry-Drained	Low	Mono
1.2	Dry-Drained	Medium	
1.3	Dry-Drained	High	
2.1	Saturated-Drained	Medium	
3.1	Dry-Drained	Medium	Cyc
4.1	Saturated-Drained	Medium	
4.2	Saturated-Undrained	Medium	

3.1 Large-deformation testing box, sand beds and considerations for undrained testing

Tests will be conducted within a long-box container with internal dimensions of 1.4 m x 0.4 m x 0.65 m. This specific chamber was developed for large-deformation studies of drag embedment anchoring (DEA), cable and pipeline ploughing problems (Sharif et al., 2024; Robinson et al., 2019).

3.2 Sand beds

Beds of HST-95 sand will be used to mimic a typical North-sea superficial deposit in which the JAS technology could be based. Its properties are detailed previously in Al-defae et al. (2013) and summarised in Section 2. HST-95 has been used extensively to study soil-structure problems at 1g and elevated-g, its mechanical properties are therefore well understood. As with the 1g tests, air-pluviation, will be used to prepare sand beds. In this instance, an aerial hopper configured with an adjustable slot will be opted for as described in Davidson (2025) and density pots will be used to confirm continuity throughout the pluviated beds.

3.3 Drainage considerations

Drainage conditions around a model soil-structure problem are typically managed by leveraging rate-dependent characteristics of the soil and can be quantified by the normalised velocity criterion (V) set out below. Practically, this involves increasing the displacement rate of the structure moving through the soil or by opting for a soil with an increasingly low coefficient of consolidation (c_v) (Finnie and Randolph, 1994) or operational coefficient of consolidation (c_h) (Lehane et al., 2020) where:

$$V = u_z \cdot D / c_h \qquad (6)$$

($V \lesssim 0.1$ – drained; $V \gtrsim 30$ – undrained).

Where D is the diameter of the penetrating/displaced object, u_z is the measured displacement rate.

Within the centrifuge, elevated-g causes upscaling of pore dissipation rates by a scale factor equal to $N = g$. For a water pore-fluid paired with relatively free-draining sand (e.g., HST-95), achieving undrained conditions would be difficult with the current actuator described in the following section. After, Robinson et al., (2019), high viscosity pore-fluid (hydroxypropyl methylcellulose, HPMC) may be used to manage fluid flow, such that undrained conditions (e.g., a $V \gtrsim 30$) can be achieved at u_z orders lower than when using a water pore-fluid. HPMC is stable (and maintains its viscosity) at high-strain levels, such as those associated with the large-deformation tests planned. It is typically considered to have no significant effect on either the shear strength/stiffness degradation or stress-strain response of sands (Robinson et al., 2019).

3.4 Tether sizing and proto-type configurations

For similitude with the 1g scaling assumptions, the centrifuge tests, at the intended acceleration level of 50g will require a diameter of ~2.72 mm. The final sizing shall be selected such to avoid marked particle or boundary interaction issues, noting its structural requirements to avoid failure at the maximum planned pretension. Relevant scaling laws used here for centrifuge testing are covered in detail by Robinson et al. (2019) and Davidson (2025).

3.4.1 Anticipated testing procedure

The set-up of the 1g tests will be replicated here; the JTA will be wished in place (WIP) in an initially vertical position (see e.g., Figure 1b) and thereafter pulled laterally at a set height from the top of the sand-bed toward the actuator. Actuation will be achieved using a Parvalux SD12-LWS high torque 220 V DC motor and gearbox, capable of applying loads equivalent to 5 kN and horizontal displacements of up to 800 mm.

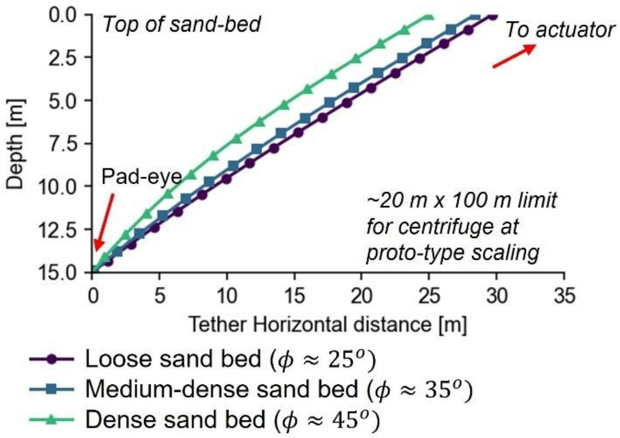

Figure 5. Approximate JTA tether profile and horizontal distance during centrifuge testing in loose to dense sand. Results estimated using Mortensen's method with a peak pretension load of 800 te applied at 25º upward from the sand bed

Provisional checks for saturated sand beds using Mortensen et al. (2015)'s framework, described in Section 0 suggests that the JTA will reach a final pretension load of (~800-1000) tonnes at a horizontal displacement of approximately 15-40 m (depending on the bed's relative density) at an angle of 25° upward from the sand-bed, as shown below in Figure 5.

Due to the fixed vertical position of the Parvalux actuator, loading angle of the JTA above the sand bed will evolve as it undergoes tensioning and cuts through the sand toward the loading point (from its initial vertical position, $\theta = 90^0$). It is believed that the testing chamber is sufficiently large such that the ultimate loading condition is achievable. The final position would be expected to fall within the semi-taut mooring-type configuration envelope, a representative scenario for the JAS.

High-level load-time sequences and their associated g-levels for both static (Phase 1-3) and cyclic (Phase 4) tests are depicted in Figure 6a and b. It is anticipated that the JTA will be initially pretensioned under elevated g to 50% of the required pretension load ($T_0 \approx 400 - 500$ te). In-flight measurements of load and displacement/angle at the pad-eye and actuator will be taken. In line with Figure 6a, the centrifuge shall then be spun down ($g = 1$) and interim inspections of the JTA will be made to confirm its profile through the sand bed before the final application of 100% pretension at elevated-g. At the end of the tests the sand bed shall be excavated for further investigation.

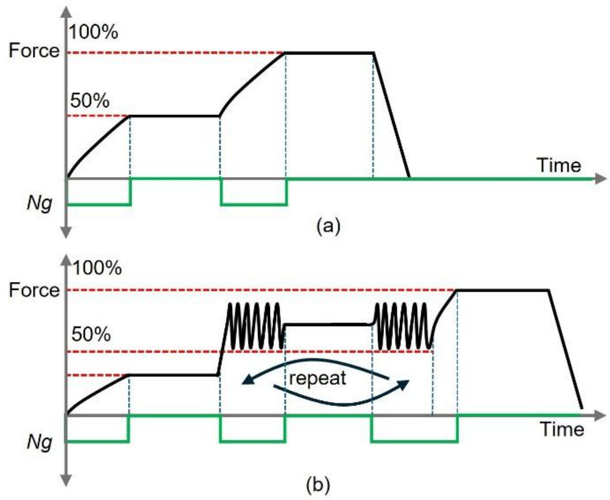

Figure 6. Typical force-time history profiles alongside associated g-levels anticipated for the centrifuge programme for: (a) static testing; and (b) cyclic testing

Cyclic load tests are planned to mimic the JTA's field-scale in-service operation. Ignoring out-of-plane loading, the system is anticipated to remain in tension under biased one-way partial cyclic loading, as schematised in Figure 6b. This bias aims to mimic repeat (e.g., fatigue limit state (FLS) type loading) and (or) abnormal/high dynamic environmental loads, which exceed the mooring's pretension load (e.g., under accidental limit state (ALS) type loading conditions; rare events exceeding 100-year returns, etc, see DNV-ST-0119 (2019)).

3.5 Conclusion

This paper has introduced a model testing campaign for soil-tether interactions. This work is supporting the development of a new anchoring technology (the Javelin Anchor System) aiming for deployment in deep waters and complex geotechnical strata, targetting floating wind renewables. In summary:

- Results from a 1:10 1g test series of the JTA (embedded mooring line) have been shared and discussed.
- Traditional bearing-capacity and CPT-based methodologies for catenary mooring assessment were compared to the 1g test series. Most methods poorly predicted the tether's overall profiles, but captured reasonably well the load shed and inclination. The reasoning was provisionally attributed to the low-effective stress levels throughout the majority of the sand bed, as well as boundary interaction close to the pad-eye. Recent CPT-based approaches incorporating tether inclination on bearing contributions are of interest here and may support refinement of the JTA sizing.
- Centrifuge scaled model tests of the JTA are plannned to be undertaken at the University of Dundee. These hope to rationalise observations made above, address any limitations around the 1g tests and extend knowledge around the system under conditions representative for the JAS deployment.
- It is planned that results from the centrifuge study will be dessiminated publically with hopes to widen the industry knowledge on embedded mooring line technologies.

4 ACKNOWLEDGEMENTS

This work was supported by government funding facilitated through BEIS/DESNZ for physical onshore testing from 2023-2025. The Cornwall and Isles of Scilly Council Good Growth Fund as part of the UK Shared Prosperity Fund are also thanked for their support.

5 REFERENCES

Al-defae, A. H., Caucis, K., & Knappett, J. A. (2013). Aftershocks and the whole-life seismic performance of granular slopes. *Géotechnique*, *63*(14), 1230–1244. https://doi.org/10.1680/geot.12.P.149

Bolton, M. D., Gui, M. W., Garnier, J., Corte, J. F., Bagge, G., Laue, J., & Renzi, R. (1999). Centrifuge cone penetration tests in sand. *Géotechnique*, *49*(4), 543–552. https://doi.org/10.1680/geot.1999.49.4.543

Brown, M., Simon-Soberon, F., & Bransby, M. (2006). The characteristics of a model pipeline plough. In *Physical Modelling in Geotechnics*. Taylor & Francis. https://doi.org/10.1201/NOE0415415866.ch101

Cerfontaine, B., White, D., Kwa, K., Gourvenec, S., Knappett, J., & Brown, M. (2023). Anchor geotechnics for floating offshore wind: Current technologies and future innovations. *Ocean Engineering*, *279*. https://doi.org/10.1016/j.oceaneng.2023.114327

Davidson, C. (2025) *Development and Installation Optimisation of Screw Piles for Offshore Wind Energy Foundation Systems*.

DNV. (2021). *DNV-ST-0119: Standard. Floating wind turbine structures.*

DNV. (2021). *DNV-RP-E302: Recommended Practice. Design and Installation of Drag-In Plate Anchors in Clay*.

Frankenmolen, S. F., White, D. J., & O'Loughlin, C. D. (2016). Chain-soil interaction in carbonate sand. *Proceedings of the Annual Offshore Technology Conference*, *3*, 2493–2519. https://doi.org/10.4043/27102-ms

GWEC. (2024). *GWEC: Global Wind Report 2024*. www.gwec.net

Gourvenec, S. (2020). Whole-life geotechnical design: What is it? What's it for? So what? and What next? *ISFOG -21*, *44*(0), 206–246.

Kwa, K. A., Evans, J. R., & White, D. J. (2024) *Station-keeping for floating offshore renewable energy: A physical modelling study of seabed-chain-anchor interactions*.

Kwa, K., O'loughlin, C., White, D., O'beirne, C., & Frankenmolen, S. (2025). Physical and theoretical modelling of embedded mooring line-seabed interaction in sands. *Geotechnique*. https://doi.org/10.1680/jgeot.24.01025

Lehane, B. M., O'loughlin, C. D., Gaudin, C., & Randolph, M. F. (2009). Rate effects on penetrometer resistance in kaolin. *Geotechnique*, *59*(1), 41–52. https://doi.org/10.1680/geot.2007.00072

Mortensen, N. (2015). Chain configuration in sand, theory and large scale field testing. In *Frontiers in Offshore Geotechnics III* (pp. 905–912). CRC Press. https://doi.org/10.1201/b18442-130

Neubecker, S. R., & Randolph, M. F. (1995). Profile and Frictional Capacity of Embedded Anchor Chains. *Journal of Geotechnical Engineering*, *121*(11), 797–803. https://doi.org/10.1061/(ASCE)0733-9410(1995)121:11(797)

Robinson, S., Brown, M. J., Matsui, H., Brennan, A., Augarde, C., Coombs, W., & Cortis, M. (2019). Centrifuge testing to verify scaling of offshore pipeline ploughs. *International Journal of Physical Modelling in Geotechnics*, *19*(6), 305–317. https://doi.org/10.1680/jphmg.17.00075

Rui, S., Guo, Z., Wang, L., Zhang, H., & Zhou, W. (2021). Axial interaction between anchor chain and sand. Part I: Monotonic loading test. *Applied Ocean Research*, *113*. https://doi.org/10.1016/j.apor.2021.102761

Sharif, Y., Brown Davidson, M. C., Coombs, W., Augarde, C., Bird, R., Carter, G., Macdonald, C., & Johnson, K. (2024). Comparison of the behaviour of a drag embedment anchor using 1-g and centrifuge scale model testing. *Proceedings of the 5th ECPMG 2024*. https://doi.org/https://doi.org/10.53243/ECPMG2024-78